University of Glasgow

Cimbri, D., Morariu, R., Ofiare, A. and Wasige, E. (2022) $In_{0.53}Ga_{0.47}As/AlAs$ Double-Barrier Resonant Tunnelling Diodes with High-Power Performance in the Low-Terahertz Band. In: 2022 Fifth IEEE International Workshop on Mobile Terahertz Systems (IWMTS), Duisburg, Germany, 04-06 Jul 2022, ISBN 9781665482752

(doi: 10.1109/IWMTS54901.2022.9832442)

This is the Author Accepted Manuscript.

© 2022 IEEE. Personal use of this material is permitted. Permission from IEEE must be obtained for all other uses, in any current or future media, including reprinting/republishing this material for advertising or promotional purposes, creating new collective works, for resale or redistribution to servers or lists, or reuse of any copyrighted component of this work in other works.

There may be differences between this version and the published version. You are advised to consult the publisher's version if you wish to cite from it.

http://eprints.gla.ac.uk/270501/

Deposited on: 9 May 2022

Enlighten – Research publications by members of the University of Glasgow
http://eprints.gla.ac.uk

$In_{0.53}Ga_{0.47}As/AlAs$ Double-Barrier Resonant Tunnelling Diodes with High-Power Performance in the Low-Terahertz Band

Davide Cimbri[1*], Razvan Morariu[1], Afesomeh Ofiare[1], and Edward Wasige[1]

[1]High-Frequency Electronics group, Division of Electronics and Nanoscale Engineering, James Watt School of Engineering, University of Glasgow, G12 8LT, Glasgow, United Kingdom

*davide.cimbri@glasgow.ac.uk

***Abstract*—In this paper, we present an $In_{0.53}Ga_{0.47}As/AlAs$ double-barrier resonant tunnelling diode (RTD) epitaxial structure that features high-power capabilities at low-terahertz frequencies ($\sim$ 100−300 GHz). The heterostructure was designed using a TCAD-based quantum transport simulator and experimentally investigated through the fabrication and characterisation of RTD devices. The high-frequency RF power performance of the epitaxial structure was analysed based on the extracted small-signal equivalent circuit parameters. Our analysis shows that a 9 μm^2, 16 μm^2, and 25 μm^2 large RTD device can be expected to deliver around 2 mW, 4 mW, and 6 mW of RF power at 300 GHz.**

***Index Terms*—Resonant tunnelling diode, epitaxial structure, small-signal modelling, terahertz.**

I. Introduction

RESONANT tunnelling diode (RTD) technology [1] offers a low-power, low-cost and compact solution suitable to design ultra-broadband wireless transceivers (TRx) for next generation high-speed terahertz (THz) (0.1−10 THz [2]) communications [3] [4]. Although indium phosphide (InP) RTD-based oscillator sources have attained output powers of up $\sim$ 1 mW at room temperature (RT) in the 300 GHz-band [5], the unoptimised epitaxial structure of the RTD device is among the main reasons that prevents from meeting the radio frequency (RF) power requirements needed for practical applications.
In this paper, we report about a lattice-matched to InP indium gallium arsenide/aluminium arsenide ($In_{0.53}Ga_{0.47}As/AlAs$) double-barrier RTD epitaxial structure with high-power performance in the low-terahertz range ($\sim$ 100−300 GHz). Based on the simulation study we reported in [6], we designed and optimised the heterostructure for high-power operation. RTD devices were fabricated and characterised to extract the associated static current density-voltage JV characteristic and small-signal equivalent circuit parameters, from which the high-frequency RF power performance of the heterostructure was investigated.

II. Proposed RTD epitaxial structure

The epitaxial structure featured an $In_{0.53}Ga_{0.47}As/AlAs$ double-barrier quantum well (DBQW) and it was designed and optimised to achieve moderate current density operation ($J_p \sim 150 - 250$ kA/cm^2), which allows the employment of large mesa areas $A \gg 1$ μm^2, low peak voltage $V_p \ll 2$ V, and large valley-to-peak voltage difference $\Delta V = V_v - V_p \gg 0.5$ V. The wafer structure was grown through molecular beam epitaxy (MBE) by Intelligent Epitaxy Technology (IntelliEPI) Inc. on a 3" semi-insulating (SI) InP substrate.

A. RTD devices fabrication

RTD devices with square top mesa area $A = 3\times3$ μm^2 were fabricated solely with optical lithography with the exception of the top contact, which was patterned through electron-beam lithography (EBL) for accurate shaping. Ohmic contacts based on a titanium/palladium/gold (Ti/Pd/Au=20/30/150 nm) metal stack and bond-pads (Ti/Au=20/400 nm) were evaporated through electron-beam physical vapour deposition (EB−PVD), while mesas were defined through anisotropic chemical wet etching (H_3PO_4:H_2O_2:H_2O=1:1:38), where the associated lateral undercut was estimated to be $\delta \simeq 3.5$ μm^2 and confirmed through scanning electron microscopy (SEM) analysis, resulting in a fabricated $A \simeq 5.5$ μm^2. Passivation and via opening were carried out using Polyimide (PI−2545) and reactive ion etching (RIE). A photomicrograph and an SEM image of a fabricated device are shown in Fig. 1.

B. RTD devices characterisation

The devices were characterised using a B1500A Semiconductor Device Parameter Analyzer from Keysight Technologies. The extracted heterostructure electrical quantities are shown in Table I, while the associated static JV characteristic is shown in Fig. 2, where $J_p \simeq 195$ kA/cm^2 = 1.95 mA/μm^2, $J_v \simeq 0.57$ mA/μm^2, $\Delta J \simeq 1.38$ mA/μm^2, PVCR $\simeq$ 3.5,

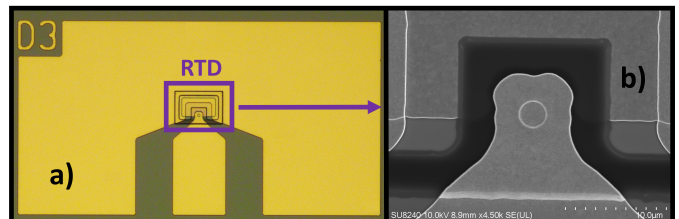

Fig. 1. In a), a photomicrograph of a fabricated RTD device. In b), an SEM image zoom in over the opened via.

TABLE I
RTD EPITAXIAL STRUCTURE ELECTRICAL QUANTITIES

J_p [mA/μm^2]	J_v [mA/μm^2]	ΔJ [mA/μm^2]	PVCR	V_p [V]	V_v [V]	ΔV [V]	G^*_{rtd} [mS/μm^2]	ν_c [THz]	C^*_{rtd} [fF/μm^2]
1.95	0.57	1.38	3.5	1.36	2.55	1.20	−3.0	4.14	5.85

* Estimated in the NDR region.

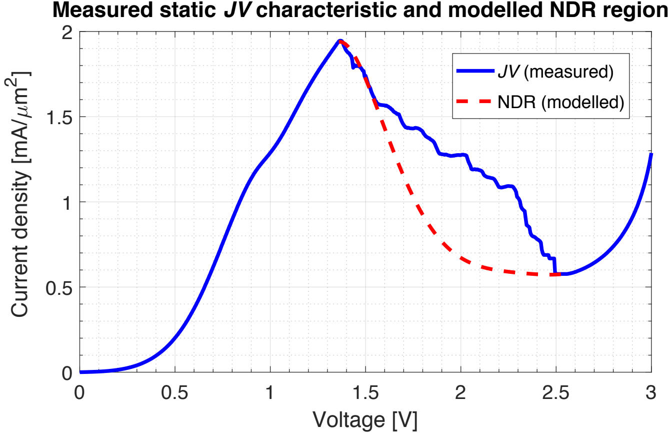

Fig. 2. Measured static JV characteristic and associated modelled NDR region of the analysed RTD heterostructure.

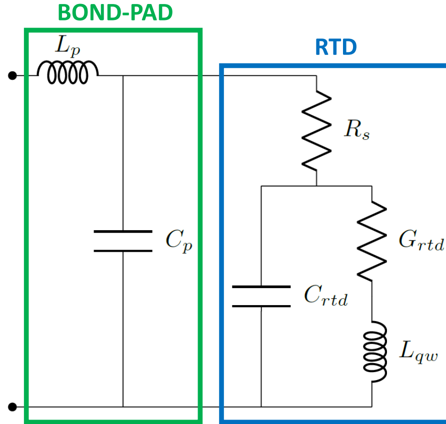

Fig. 3. RTD device and bond-pad small-signal equivalent circuit.

$V_p \simeq 1.36$ V, $V_v \simeq 2.55$ V, and $\Delta V \simeq 1.2$ V.

To determine the high-frequency performance of the proposed epitaxial structure, an estimate of the capacitance C_{rtd} is also required, where $C_{rtd} \approx C_d + C_{qw}$ [7], where $C_d = \epsilon_{rtd}/t_{rtd}$ is the depletion capacitance (being ϵ_{rtd} and t_{rtd} the equivalent dielectric constant and thickness associated with the heterostructure depletion regions, respectively) and $C_{qw}(V) = G_{rtd}(V)/\nu_c$ is the quantum capacitance (being G_{rtd} the differential conductance and ν_c the electron escape rate from the quantum well (QW) to the collector, which is assumed bias independent), on-wafer one-port S-parameters measurement was carried out after accurate calibration in the frequency range 10 MHz−110 GHz using an E8361A PNA vector network analyser (VNA) working in the frequency range 10 MHz−67 GHz, an N5250 millimetre head controller, and frequency extenders N5262A working between 67−110 GHz, all from Keysight Technologies. A coplanar waveguide design with characteristic impedance $Z_0 = 50\ \Omega$ was adopted to realise the RTD bond-pads in order to match with the employed RF ground-signal-ground (GSG) probe from GGB Industries Inc., featuring 100 μm pitch.

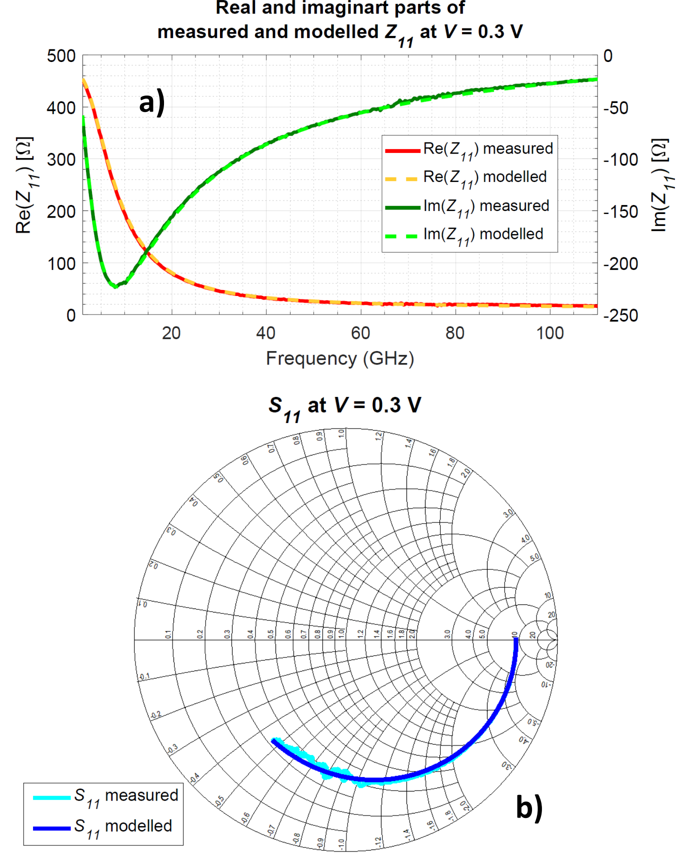

Fig. 4. In a), measured and modelled real and imaginary parts of Z_{11} in the frequency range 10 MHz−110 GHz at $V = 0.3$ V. In b), measured and modelled S_{11} in the frequency range 10 MHz−110 GHz at $V = 0.3$ V.

TABLE II
RTD DEVICE AND BOND-PAD SMALL-SIGNAL PARAMETERS AT V = 0.3 V

C_p [fF]	L_p [pH]	R_s [Ω]	G_{rtd} [mS]	C_{rtd} [fF]	L_{qw} [nH]
17.5	20.8	42.1	2.4	27.3	0.13

TABLE III
EPITAXIAL STRUCTURE HIGH-FREQUENCY RF POWER PERFORMANCE

τ_{dbqw} [ps]	τ_t [fs]	τ_{in} [ps]	f_i [THz]	$P_{RF,max}$	P_{RF} (100 GHz)	P_{RF} (200 GHz)	P_{RF} (300 GHz)
0.24	14	0.25	1.39	0.31 mW/μm^2	0.31 mW/μm^2	0.30 mW/μm^2	0.29 mW/μm^2
ρ_c [Ω μm^2]	f_{max} [GHz]	τ_{rtd} [ps]	f_c [GHz]	$P_{RF,max}$	P_{RF} (100 GHz)	P_{RF} (200 GHz)	P_{RF} (300 GHz)
13	405	0.63	396	0.31 mW/μm^2	0.29 mW/μm^2	0.22 mW/μm^2	0.12 mW/μm^2
8	520	0.51	493	0.31 mW/μm^2	0.30 mW/μm^2	0.25 mW/μm^2	0.18 mW/μm^2
2	1050	0.30	840	0.31 mW/μm^2	0.31 mW/μm^2	0.29 mW/μm^2	0.26 mW/μm^2

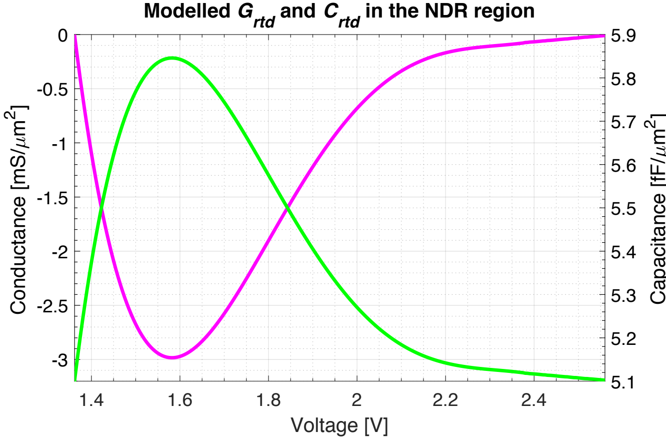

Fig. 5. Modelled (negative) differential conductance G_{rtd} and capacitance C_{rtd} in the NDR region of the analysed heterostructure.

Since the devices exhibited instability within the negative differential resistance (NDR) region due to low-frequency parasitic oscillations caused the bias line inductance, the extraction was carried out following the approach described in [8]. First, S-parameters were measured in both the first and second positive differential resistance (PDR) regions to extract ν_c. To do that, a small-signal model, including the bond-pad and the RTD device, was employed, which is depicted in Fig. 3, and comprised of the bond-pad inductance L_p and capacitance C_p, and the RTD series resistance $R_s \approx R_c$ (where R_c is the Ohmic contacts resistance), differential conductance G_{rtd}, capacitance C_{rtd}, and QW inductance L_{qw}. The bond-pad resistance R_p was omitted since negligible (estimated to be $\simeq$ 0.2 Ω). The model was imported in Advance Design System (ADS) from Keysight Technologies and the measured S_{11} and converted Z_{11} parameters fitted at different bias points. An example of fitting at $V = 0.3$ V is shown in Fig. 4, while the associated extracted small-signal parameters are reported in Table II, where $C_p \simeq 17.5$ fF, $L_p \simeq 20.8$ pH, $R_s \simeq 42.1$ Ω, $G_{rtd} \simeq 2.4$ mS, $C_{rtd} \simeq 27.3$ fF, and $L_{qw} \simeq 0.13$ nH. The extracted C_d and ν_c were $\simeq 5.1$ fF/μm^2 and $\simeq 4.14$ THz, respectively, after correcting with the parasitic capacitance associated with the passivation layer, which was estimated to be $\simeq 1.6$ fF for the fabricated RTD devices.

The NDR region of the static JV characteristic was then modelled through a 6th-order polynomial function to retrieve $G_{rtd} = dJ/dV$, as shown in Fig. 2, and C_{rtd} was then finally extracted, as shown in Fig. 5. Good match between modelled and measured G_{rtd} values at the analysed PDR bias points was met. The estimated G_{rtd} and C_{rtd} in the NDR region were $\simeq -3.0$ mS/μm^2 and $\simeq 5.85$ fF/μm^2, respectively.

C. RF power analysis

Table III shows the high-frequency RF power performance of the proposed RTD epitaxial structure. The intrinsic response frequency limit f_i [9]:

$$f_i \approx \frac{1}{4\tau_{in}} \tag{1}$$

was estimated to be $\simeq 1.39$ THz, where $\tau_{in} = \tau_{dbqw} + \tau_t/2$ is the electron total intrinsic delay time across the RTD heterostructure [12], τ_{dbqw} is the tunnelling time across the DBQW region, which was estimated to be $\simeq 0.24$ ps from the simulated transmission coefficient resonant peak full-width at half maximum (FWHM) energy broadening $\Gamma_1 \simeq 3.8$ meV of the first quasi-bound state energy level E_1, which is shown in Fig. 6, while τ_t is the transit time across the depletion regions, where $\tau_t/2$ was estimated to be $\simeq 7$ fs assuming the

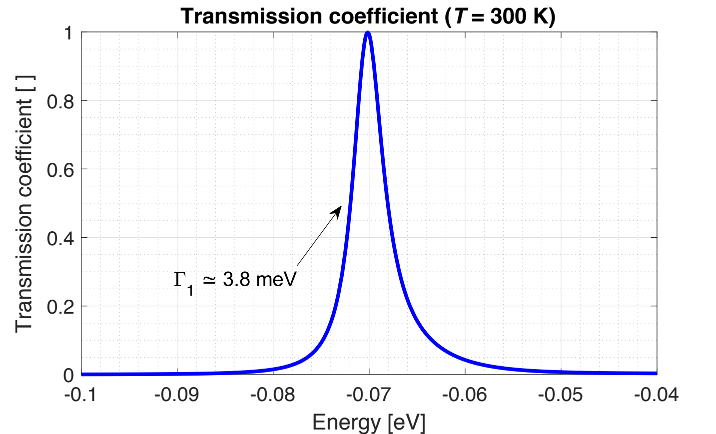

Fig. 6. Simulated transmission coefficient resonant peak associated with E_1 at room temperature ($T = 300$ K), outlining the related energy broadening $\Gamma_1 \simeq 3.8$ meV.

TABLE IV
RTD HIGH-FREQUENCY RF POWER PERFORMANCE

ρ_c [Ω μm^2]	A [μm^2]	$P_{RF,max}$ [mW]	P_{RF} (f_{op} = 100 GHz) [mW]	P_{RF} (f_{op} = 200 GHz) [mW]	P_{RF} (f_{op} = 300 GHz) [mW]
13	9	2.8	2.6	2.0	1.1
	16	5.0	4.6	3.5	1.9
	25	7.8	7.3	5.5	3.0
8	9	2.8	2.7	2.3	1.6
	16	5.0	4.8	4.0	2.9
	25	7.8	7.5	6.3	4.5
2	9	2.8	2.8	2.6	2.3
	16	5.0	5.0	4.6	4.2
	25	7.8	7.8	7.3	6.5

$In_{0.53}Ga_{0.47}As$ electron saturation velocity $v_{e,s} \sim 3\times10^7$ cm/s [9], giving a total $\tau_{in} \simeq 0.25$ ps.
While the maximum RF power $P_{RF,max}$ is given by [10]:

$$P_{RF,max} \approx \frac{3}{16}\Delta J \Delta V \tag{2}$$

and was estimated to be $\simeq 0.31$ mW/μm^2, the RF power at high-frequency P_{RF} can be approximated as [11]:

$$P_{RF} \approx P_{RF,max}\, cos(2\pi f_{op}\tau_{in}) \tag{3}$$

(being f_{op} the operation frequency) which is shown in Fig. 7, and was estimated to be $\simeq 0.31$ mW/μm^2, $\simeq 0.30$ mW/μm^2, and $\simeq 0.29$ mW/μm^2 at $f_{op} = 100$ GHz, 200 GHz, and 300 GHz, respectively.
The cut-off frequency limit of the RTD device due to external parasitics can be modelled through the extrinsic delay time τ_{ex}, which can be approximated as [12]:

$$\tau_{ex} \approx \frac{\pi C_{rtd}}{2}\sqrt{\frac{\rho_c}{G_{rtd}}} \tag{4}$$

being $\rho_c = R_c A$, where A is the RTD top mesa area and $R_c = R_{c,t} + R_{c,b} = \rho_c/(A + A_b)$ (being $R_{c,t}$ and $R_{c,b}$ the contact resistances associated with the RTD top and bottom Ohmic contacts, respectively, while A_b is the bottom contact area), where $R_c \approx R_{c,t}$ since the ratio $R_{c,t}/R_{c,b} = A_b/A$ was estimated to be ~ 22 for the fabricated devices. In this context, the device maximum oscillation frequency f_{max} can be approximated as [13]:

$$f_{max} \approx \frac{1}{4\tau_{ex}} \approx \frac{G_{rtd}}{2\pi C_{rtd}}\sqrt{\frac{1}{R_s G_{rtd}} - 1} \tag{5}$$

Although no pre-evaporation surface de-oxidation was carried out in this work during Ohmics fabrication, where the extracted ρ_c was $\simeq 202$ Ω μm^2 from the measured S-parameters, simple cleaning procedures can lead to $\rho_c \simeq 13$ Ω μm^2 [14], while optimised approaches can lower it down to $\simeq 1$ Ω μm^2 [15] employing the same metal stack. For instance, τ_{ex} was estimated to be $\simeq 0.60$ ps, $\simeq 0.47$ ps, and $\simeq 0.24$ ps assuming $\rho_c = 13$ Ω μm^2, 8 Ω μm^2, and 2 Ω μm^2, respectively, which correspond to $f_{max} \simeq 405$ GHz, $\simeq 520$ GHz, and $\simeq 1.05$ THz, respectively.

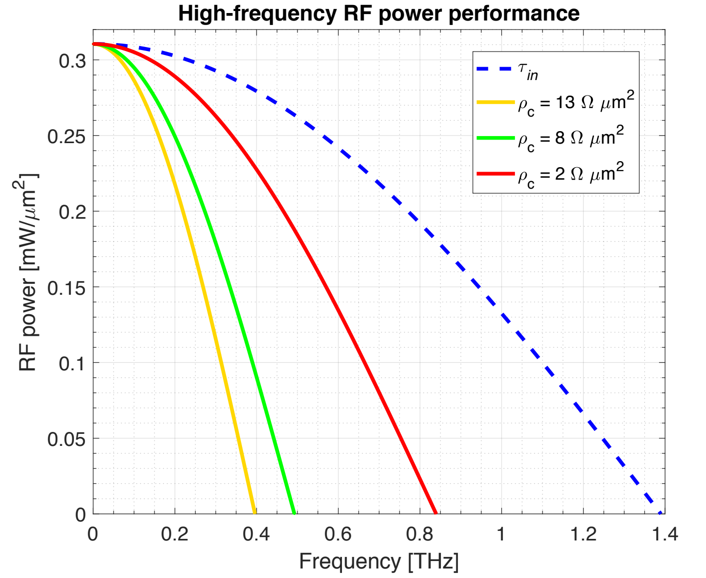

Fig. 7. RF power versus operation frequency f_{op} of the proposed RTD heterostructure .

The total delay time τ_{rtd} due to both intrinsic and extrinsic contributes is then given by [12]:

$$\tau_{rtd} = \sqrt{\tau_{in}^2 + \tau_{ex}^2} \tag{6}$$

and was estimated to be $\simeq 0.63$ ps, $\simeq 0.51$ ps, and $\simeq 0.30$ ps assuming $\rho_c = 13$ Ω μm^2, 8 Ω μm^2, and 2 Ω μm^2, respectively, which correspond to cut-off frequencies f_c [9]:

$$f_c \approx \frac{1}{4\tau_{rtd}} \tag{7}$$

of $\simeq 396$ GHz, $\simeq 493$ GHz, and $\simeq 840$ GHz, respectively.
The high-frequency RF power performance of the RTD heterostructure is therefore given by:

$$P_{RF} \approx P_{RF,max}\, cos(2\pi f_{op}\tau_{rtd}) \tag{8}$$

and was estimated to be $\simeq 0.29$ mW/μm^2, $\simeq 0.22$ mW/μm^2, and $\simeq 0.12$ mW/μm^2 with $\rho_c = 13$ Ω μm^2, $\simeq 0.30$ mW/μm^2, $\simeq 0.25$ mW/μm^2, and $\simeq 0.18$ mW/μm^2 with $\rho_c = 8$ Ω μm^2, and $\simeq 0.31$ mW/μm^2, $\simeq 0.29$ mW/μm^2, and $\simeq 0.26$ mW/μm^2

with $\rho_c = 2\ \Omega\ \mu\text{m}^2$ at $f_{op} = 100$ GHz, 200 GHz, and 300 GHz, respectively, as shown in Fig. 7.
Table IV shows the RF power performance at high-frequency of RTD devices with different mesa area and for different ρ_c values employing the proposed epitaxial structure. Based on the aforementioned analysis, 9 μm^2, 16 μm^2, and 25 μm^2 large devices can provide RF powers of up to $\simeq$ 2.8 mW, $\simeq$ 5.0 mW, and $\simeq$ 7.8 mW at $f_{op} = 100$ GHz, $\simeq$ 2.6 mW, $\simeq$ 4.6 mW, and $\simeq$ 7.3 mW at $f_{op} = 200$ GHz, and $\simeq$ 2.3 mW, $\simeq$ 4.2 mW, and $\simeq$ 6.5 mW at $f_{op} = 300$ GHz, respectively.

III. Conclusions

In this work, we designed and experimentally investigated a proposed high-power $In_{0.53}Ga_{0.47}As$/AlAs RTD epitaxial structure. The RF power performance of the epi-layer was analysed through the extracted small-signal parameters of the fabricated and measured RTD devices. Results indicate that a 9 μm^2, 16 μm^2, and 25 μm^2 large device can be expected to deliver an RF power in excess of 2 mW, 4 mW, and 6 mW at 300 GHz. Future work will focus on the employment of the proposed or similar heterostructures to realise oscillator sources and investigate the associate output power performance at low-THz frequencies.

IV. Acknowledgments

The authors would like to thank the James Watt Nanofabrication Centre (JWNC) staff, University of Glasgow, for the support during devices fabrication. The work of Davide Cimbri was supported by TeraApps (Doctoral Training Network in Terahertz Technologies for Imaging, Radar and Communication Applications), which received funding from the European Union's Horizon 2020 research and innovation programme under Marie Skłodowska-Curie Innovative Training Network (ITN) grant agreement No. 765426.

References

[1] M. Feiginov, "Frequency Limitations of Resonant-Tunnelling Diodes in Sub-THz and THz Oscillators and Detectors," *Journal of Infrared, Millimeter, and Terahertz Waves*, vol. 40, no. 4, pp. 365-394, 2019, doi: 10.1007/s10762-019-00573-5.

[2] T. Nagatsuma, "Terahertz technologies: present and future," *IEICE Electronics Express*, vol. 8, no. 14, pp. 1127-1142, 2011, doi: 10.1587/elex.8.1127.

[3] D. Cimbri, J. Wang, A. Al-Khalidi, and E. Wasige, "Resonant Tunnelling Diode High-Speed Terahertz Wireless Communications - A Review," *IEEE Transactions on Terahertz Science and Technology*, vol. 12, no. 3, pp. 226-244, 2022, doi: 10.1109/TTHZ.2022.3142965.

[4] H. -J. Song and T. Nagatsuma, "Present and Future of Terahertz Communications," *IEEE Transactions on Terahertz Science and Technology*, vol. 1, no. 1, pp. 256-263, 2011, doi: 10.1109/TTHZ.2011.2159552.

[5] A. Al-Khalidi, K. H. Alharbi, J. Wang, R. Morariu, L. Wang, A. Khalid, J. M. L. Figueiredo, and E. Wasige, "Resonant Tunneling Diode Terahertz Sources With up to 1 mW Output Power in the J-Band," *IEEE Transactions on Terahertz Science and Technology*, vol. 10, no. 2, pp. 150-157, 2020, doi: 10.1109/TTHZ.2019.2959210.

[6] D. Cimbri, J. Wang, and E. Wasige, "Epitaxial Structure Simulation Study of $In_{0.53}Ga_{0.47}As$/AlAs Double-Barrier Resonant Tunnelling Diodes," *2022 Fifth International Workshop on Mobile Terahertz Systems (IWMTS)*, Duisburg-Essen, 4-6th July 2022 (accepted for publication).

[7] Q. Liu, A. Seabaugh, P. Chahal, and F. J. Morris, "Unified AC model for the resonant tunneling diode," *IEEE Transactions on Electron Devices*, vol. 51, no. 5, pp. 653-657, 2004, doi: 10.1109/TED.2004.825795.

[8] R. Morariu, J. Wang, A. C. Cornescu, A. Al-Khalidi, A. Ofiare, J. M. L. Figueiredo, and E. Wasige, "Accurate Small-Signal Equivalent Circuit Modeling of Resonant Tunneling Diodes to 110 GHz," *IEEE Transactions on Microwave Theory and Techniques*, vol. 67, no. 11, pp. 4332-4340, 2019, doi: 10.1109/TMTT.2019.2939321.

[9] M. Asada, S. Suzuki, and N. Kishimoto, "Resonant Tunneling Diodes for Sub-Terahertz and Terahertz Oscillators," *Japanese Journal of Applied Physics*, vol. 47, no. 6R, pp. 4375-4384, 2008, doi: 10.1143/JJAP.47.4375.

[10] C. Kim and A. Brandli, "High-Frequency High-Power Operation of Tunnel Diodes," *IRE Transactions on Circuit Theory*, vol. 8, no. 4, pp. 416-425, 1961, doi: 10.1109/TCT.1961.1086849.

[11] S. Suzuki, M. Shiraishi, H. Shibayama, and M. Asada, "High-Power Operation of Terahertz Oscillators With Resonant Tunneling Diodes Using Impedance-Matched Antennas and Array Configuration," *IEEE Journal of Selected Topics in Quantum Electronics*, vol. 19, no. 1, pp. 8500108-8500108, 2013, doi: 10.1109/JSTQE.2012.2215017.

[12] H. Kanaya, T. Maekawa, S. Suzuki, and M. Asada, "Structure dependence of oscillation characteristics of resonant-tunneling-diode terahertz oscillators associated with intrinsic and extrinsic delay times," *Japanese Journal of Applied Physics*, vol. 54, no. 9, pp. 094103, 2015, doi: 10.7567/JJAP.54.094103.

[13] E. R. Brown, C. D. Parker, and T. C. L. G. Sollner, "Effect of quasibound-state lifetime on the oscillation power of resonant tunneling diodes," *Applied Physics Letters*, vol. 54, no. 10, pp. 934-936, 1989, doi: 10.1063/1.100812.

[14] D. Cimbri, N. Weimann, Q. R. A. Al-Taai, A. Ofiare, and E. Wasige, "Ohmic Contacts Optimisation for High-Power InGaAs/AlAs Double-Barrier Resonant Tunnelling Diodes Based on a Dual-Exposure E-Beam Lithography Approach," *International Journal of Nanoelectronics and Materials*, vol. 14 (Special Issue), pp. 11-19, Proceedings of the 3rd International Conference on Applied Photonics and Electronics (InCAPE), Perlis, 6th October 2021.

[15] A. M. Crook, E. Lind, Z. Griffith, M. J. W. Rodwell, J. D. Zimmerman, A. C. Gossard, and S. R. Bank, "Low resistance, nonalloyed Ohmic contacts to InGaAs," *Applied Physics Letters*, vol. 91, no. 19, pp. 192114, 2007, doi: 10.1063/1.2806235.